A Step Towards Learning Contraction Kernels for Irregular Image Pyramid

Darshan Batavia[1][a], Rocio Gonzalez-Diaz[2][b] and Walter G. Kropatsch[1][c]
[1]*TU Wien, Pattern Recognition and Image Processing Group 193/03, Vienna, Austria*
[2]*University of Seville, Department of Applied Math I, Seville, Spain*

Keywords: Cost of Contraction Kernels, Dictionary for Contraction Kernel, Irregular Image Pyramid, Slope Region.

Abstract: A structure preserving irregular image pyramid can be computed by applying basic graph operations (contraction and removal of edges) on the 4-adjacent neighbourhood graph of an image. In this paper, we derive an objective function that classifies the edges as contractible or removable for building an irregular graph pyramid. The objective function is based on the *cost* of the edges in the contraction kernel (sub-graph selected for contraction) together with the size of the contraction kernel. Based on the objective function, we also provide an algorithm that decomposes a 2D image into monotonically connected regions of the image surface, called slope regions. We proved that the proposed algorithm results in a graph-based irregular image pyramid that preserves the structure and the topology of the critical points (the local maxima, the local minima, and the saddles). Later we introduce the concept of the dictionary for the connected components of the contraction kernel, consisting of sub-graphs that can be combined together to form a set of contraction kernels. A favorable contraction kernel can be selected that best satisfies the objective function. Lastly, we show the experimental verification for the claims related to the objective function and the cost of the contraction kernel. The outcome of this paper can be envisioned as a step towards learning the contraction kernel for the construction of an irregular image pyramid.

1 INTRODUCTION

Graph-based representations are the primary object of study for many pattern recognition and computer vision application areas. Graphs are capable of representing both structured and unstructured data associated with applications ranging from processing 2D images to social network analysis and climate data analysis. Out of several approaches to encounter graph-based processing, this paper focuses on the construction of an irregular image pyramid computed from a 2D image, such that the topology and the structure of the image are preserved blue in a concise manner at the higher levels of the pyramid. The proposed objective function is used to predict an optimal contraction kernel that governs the construction of an irregular image pyramid. In the broader context, the proposed algorithm decomposes a 2D Euclidean space into cells that are represented by critical points (the local maximum, the local minimum, and the saddle) and the connections between them. As mentioned in (Helman and Hesselink, 1991), a compact representation of a 2D image can be achieved by using a surface topology-based data structure.

There is an extensive literature on similar approaches for the decomposition of the 2D spaces, especially for the decomposition of the Morse-Smale complex (MS-complex). As mentioned in (Stein et al., 1963), the Morse-Smale complex is a collection of the Morse cells that follow a smooth function on a manifold, $h : \mathbb{M} \mapsto \mathbb{R}$ such that all the critical points are non-degenerated. Nackman Lee in (Lee, 1984) represents a surface in form of graphs of critical points, subdividing the surface into slope districts. Other approaches include: Reeb graph (Shinagawa et al., 1991), hierarchical decomposition of MS-complex into piece-wise linear 2-manifolds (Edelsbrunner et al., 2003). Many efficient algorithms can be found in the literature to compute consistent MS complexes. For example, in (Gyulassy et al., 2014), the authors presented an efficient algorithm to compute consistent MS complexes using

[a] https://orcid.org/0000-0003-0062-3411
[b] https://orcid.org/0000-0001-9937-0033
[c] https://orcid.org/0000-0003-4915-4118

a divide-and-conquer strategy for dealing with large data. In (Comic et al., 2010), the authors computed maximal cells of the ascending and the descending Morse complexes through a watershed approach.

In reality, 2D images may contain degenerated critical points and thus they cannot be treated as MS-complexes before any pre-processing. Therefore, in this paper, we focus on a more generic framework that allows the presence of degenerated critical points. In (Gonzalez-Diaz et al., 2021), the authors explained a hierarchical approach for the decomposition of any surface into cells called *slope regions* and proved the necessary and sufficient conditions for the existence of the slope regions. The authors in (Batavia et al., 2019) described the partitioning of an image into slope regions. Utilizing these theories, in (Batavia et al., 2020), the authors used the combinatorial pyramid framework to build irregular image pyramids and displayed results for over-segmented images and image reconstruction from the top level of the graph pyramid while preserving the texture information. A similar framework were used by Morales-Gonzalez et al. in (Morales-González and García-Reyes, 2013) for the application of object recognition and object matching.

The main goal of this paper is to express the algorithm mentioned in (Batavia et al., 2020) for irregular image pyramid in form of an objective function and introduce the dictionary for the connected components of the contraction kernel. The paper is organized as follows: Section 2 introduces and defines the basic terminology and the motivation behind this work. Then, we derive the objective function and explain the algorithm for building the irregular image pyramid. In Section 4, we show a novel concept of a dictionary for the connected components of the contraction kernel, consisting of a generic set of subgraphs that can be used in combination to construct a favorable contraction kernel. Experimental verification and statistical evidences are shown in Section 5 for the claims made in Section 3. Then, we conclude the paper with the conclusions and the future work.

2 DEFINITIONS AND MOTIVATION

A 2D image P can be visually perceived as a sampled version of a geographical terrain model in 2.5D with a continuous height (intensity) map $h : \mathbb{R}^2 \rightarrow [0,1]$. A pixel $p \in P$ is a discrete sample obtained by sampling the 2.5D continuous surface. The digital image P can be effectively represented by a planar 4-connected neighbourhood graph $G_0 = (V_0, E_0)$, where every pixel p in the image P corresponds to a vertex $v \in V_0$ with gray value $g(v) := h(p) \in [0,1]$.

With help of basic graph operations, namely the edge contraction and the edge removal, we can reduce the graph size. Stacking up the reduced graphs will result in a formation of an irregular graph pyramid. The k^{th} level of an irregular graph pyramid is denoted by $G_k(V_k, E_k)$ where V_k and E_k are the set of vertices and edges respectively, and $k \in \{0,1,\ldots,n\}$ outlines the level of the graph pyramid. $|E_k|$ and $|V_k|$ denotes the cardinality of the edge set E_k and of the vertex set V_k, respectively.

For each edge $(v,w) \in E_k$, where $v,w \in V_k$, there is an attribute *contrast* $c(e) := |g(v) - g(w)|$. The edges are oriented from vertex v to vertex w if $g(v) > g(w)$, if $g(v) = g(w)$ they are non-oriented. A connected sub-graph of G_k having the same gray value for all the vertices is referred to as a *plateau region* (connected sub-graph of degenerated vertices). A *path* $\pi(v_1, v_2, \ldots, v_r) = (V_\pi, E_\pi)$ is defined as a nonempty sub-graph of $G_k(V_k, E_k)$, where $V_\pi = \{v_1, v_2, \ldots, v_r\} \subseteq V_k$ and $E_\pi = \{(v_1, v_2), (v_2, v_3), \ldots, (v_{r-1}, v_r)\} \subseteq E_k$. The path π is *monotonic* if all the oriented edges of E_π have the same orientation, i.e. from v_1 to v_r or from v_r to v_1. The path π is a *level curve* if $g(v_i) = g(v_{i+1}), \forall i \in \{1,2,\ldots,r-1\}$. A level curve can be a part of a monotonic path.

We utilize the orientation of the incident edges to categorize the vertices into critical vertices (local maxima, local minima, and saddles), and non-critical (slope) vertices. A vertex $v \in V_k$ is a *local minimum* if all the edges incident to v are oriented inward. A vertex $v \in V_k$ is a *local maximum* if all the edges incident to v are oriented outward. A vertex $v \in V_k$ is a *slope vertex* (non-critical vertex) if there are exactly two changes in the orientation of edges incident to v, when traversed circularly (clockwise or anti-clockwise direction). A vertex $v \in V_k$ is a *saddle* if it is not a local maximum, nor a local minimum, neither a slope vertex.

A 2D image is called *well-composed* (Latecki et al., 1995) if it does not contain the following *non-well-composed* configuration of pixels as shown in the left image of Fig.1. The non-well-composed configuration follows: $g(a) < g(b), g(a) < g(d), g(c) < g(b)$ and $g(c) < g(d)$ visualized with the help of oriented edges in Fig.1.

In order to remove all the non-well-composed configurations, we insert the hidden saddle as a vertex r adjacent to vertices a,b,c and d such that $max(g(a), g(c)) < g(r) < min(g(b), g(d))$ as shown in the right picture of Fig.1. A face in a surface embedded plane graph G_k is a *slope region* $\mathbb{S}$ if all the pairs

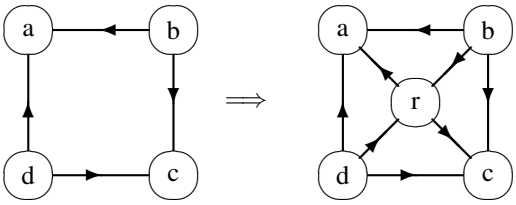

Figure 1: Inserting a hidden saddle.

of points in the face can be connected by a continuous monotonic curve inside the face. In (Batavia et al., 2019), the authors showed that a surface sampled by a 2D image can be partitioned into slope regions while preserving the structural and topological properties of the surface. Following are the basic properties and advantages of slope regions:

1. Slope regions have an easy graph-based representation comprising of one local maximum, one local minimum, and the saddle vertices along the slope's boundary connected by monotonic paths or level curves only.
2. The holes that are geometrically inside the slope region can be modeled with the help of folded boundaries, such that the holes are topologically excluded and the slope region remain homeomorphic to a disc. Please refer (Batavia et al., 2019) for further details.
3. There is no unique solution for partitioning an image into a combination of slope regions. This provides flexibility and scope for optimization to achieve better application-specific results.
4. Unlike most machine learning approaches, the slope regions can be computed without the computation of convolutions.

Motivation: The authors in (Batavia et al., 2020) implemented the TIIP (Topology preserving Irregular Image Pyramid) algorithm for the construction of an irregular image pyramid that partitions the image into slope regions while preserving the structure of an image. The main contribution of the TIIP algorithm is the selection criteria for the contraction kernel that dominates the construction of an irregular pyramid. The TIIP algorithm follows a well-defined set of rules that can be fulfilled by several implementation approaches. Therefore the modifications related to the application-specific optimizations require a deep understanding of the implementation. To avoid these drawbacks, in this paper, we derive an objective function to replicate the TIIP algorithm and to optimize the selection of contractible edges that satisfy the basic rules of selection of contraction kernel mentioned in (Batavia et al., 2020). Furthermore, we design a dictionary of sub-graphs whose elements can be combined to form a favourable contraction kernel. Alternatively, a favorable kernel can be selected from a set of contraction kernels by computing the cost of the kernels using the cost curve defined later in this paper. The outcome of this paper can be envisioned as a step towards learning the contraction kernel for an irregular graph pyramid.

3 DERIVING THE OBJECTIVE FUNCTION

As mentioned previously, the construction of an irregular pyramid is controlled by a contraction kernel $\mathcal{K}$. A **contraction kernel** $\mathcal{K} = \{e_i \in E_k : i \in \{1,2,...,n\}\}$ is a set of edges selected for the contraction. A contraction kernel $\mathcal{K}$ is accompanied with a set of **surviving vertices** $\mathcal{S} = \{v_i \in V_k : i \in \{1,2,...,n\}\}$ is a set of surviving vertices where vertex v_i corresponds to edge $e_i \in \mathcal{K}$ for $i \in \{1,2,...,n\}$. The set of surviving vertices avoids the confusion of the surviving and the non-surviving vertex during the contraction of an edge. Every contraction of an edge removes one edge and one vertex. The contraction kernel $\mathcal{K}$ is composed of several connected components denoted by C_i; $i = \{1,2,...,c\}$. Note that each connected component C_i has a single surviving vertex. The cardinality $|C_i|$ of a connected component C_i is defined as the number of edges in the connected component. Then, the **cardinality of the contraction kernel** $\mathcal{K}$ is $|\mathcal{K}| := n = \sum_{i=1}^{c} |C_i|$.

In this section, we aim to derive the objective function that replicates the rules for selecting the contraction kernels mentioned in (Batavia et al., 2020; Gonzalez-Diaz et al., 2021). Following are the basic rules mentioned in (Batavia et al., 2020) for determining a contraction kernel $\mathcal{K}$ to build a topology-preserving irregular image pyramid partitioning an image into slope regions:

1. The edges with lower contrast will be given priority over the edges with higher contrast.
2. To allow parallel processing, the connected components of the contraction kernel should be independent of each other, considering the data structure in effect.
3. The critical vertices should always survive and the edges connecting two critical vertices should be excluded from the contraction.

Further rules can be added depending on the application and the requirements from the output. Since

these rules are incomprehensible by the machines, they are manually programmed which restricts further modification and optimization. The following objective function tries to capture the above-mentioned rules, making them understandable to machines.

The objective function stated in this paper operates on the cost $\xi(e)$ associated with an edge e. Hence, before diving into the objective function, we will define the cost $\xi(e) \rightarrow [0,1]$ associated with an edge $e \in E_k$ as follows:

$$\xi(e) = 1 - \exp\left(m \cdot \ln\left(1 - c(e)\right)\right) \tag{1}$$

where $c(e) \in [0,1]$ corresponds to the contrast of an edge $e \in E_k$ and the **multiplier** m satisfies $m > 0$. The multiplier m controls the skewness of the curve $\xi(e)$ vs. $c(e)$ as shown in Fig. 2, with different values of multiplier m. The cost $\xi(e)$ associated with an edge e is proportional to the contrast $c(e)$. The cost $\xi(e)$ is bounded between $[0,1]$ for the different values of $c(e)$ as follows:

$$\begin{array}{ll} \xi(e) = 0 & \text{for } c(e) = 0 \\ \xi(e) = 1 & \text{for } c(e) = 1 \\ \xi(e) \in (0,1) & \text{for } 0 < c(e) < 1 \end{array} \tag{2}$$

The value of the multiplier m adds a non-linear factor to the cost of the edges. As displayed in Fig.2, the cost of edges with contrast ranging between $(0,1)$ is significantly lower for $m = 0.25$ as compared to the cost with multiplier $m = 1$. The maximum and the minimum value of the cost $\xi(e)$ remains unaffected by different values of the multiplier m.

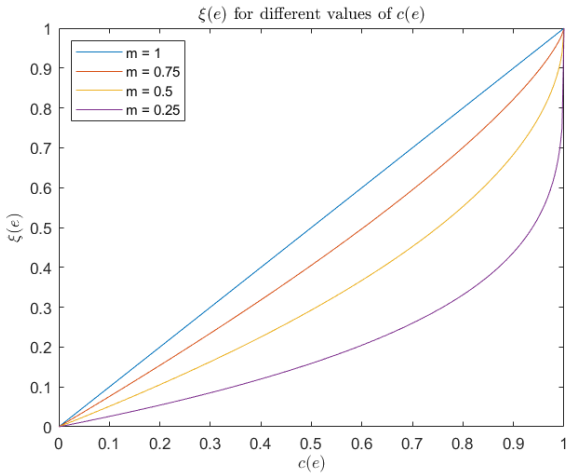

Figure 2: $\xi(e)$ vs. $c(e) = [0,1]$ for different values of m.

The cost curve $\beta(\mathcal{K}) \mapsto \mathbb{R}^+$ provides the cost associated with a contraction kernel $\mathcal{K} = \{e_j \in E_k : j \in \{1,2,...,|\mathcal{K}|\}\}$ for the k^{th} level of the graph pyramid $G_k(E_k, V_k)$:

$$\beta(\mathcal{K}) = \sum_{j=1}^{|\mathcal{K}|} \xi(e_j) + \lambda\left(\frac{|E_k| - |\mathcal{K}|}{|E_k|}\right) \tag{3}$$

The first term in Equation (3) computes the sum of the cost associated with all the edges $e_j \in \mathcal{K}$. From Equation (2), the range of the first term $\sum_{j=1}^{|\mathcal{K}|} \xi(e_j)$ is bounded between $[0, |\mathcal{K}|]$. The second half of the Equation (3) assists in controlling the kernel size. Further significance of the second term is made evident in the explanation of the following objective function.

Given a set of all the possible contraction kernels $\mathbb{S} = \{\mathcal{K}^1, \mathcal{K}^2, \ldots, \mathcal{K}^n\}$. The contraction kernel $\hat{\mathcal{K}} \in \mathbb{S}$ that helps to select the edges with lower contrast and a favorable size of contraction kernel is given by:

$$\hat{\mathcal{K}} = \arg\min_{\mathcal{K}^i \in \mathbb{S}} \beta(\mathcal{K}^i) \tag{4}$$

In Equation (4) we have two parameters: multiplier m and the Lagrange multiplier λ as shown in Equations (1,3). From Fig. 2, we can observe that the edges with a lower contrast have a smaller cost as compared to the edges with the higher contrast. Hence by minimizing the objective function in Equation (4), we are giving priority to the edges with the lower contrast, satisfying the rule mentioned in (Batavia et al., 2020). The Lagrange multiplier λ penalizes the size of the contraction kernel. The size of the contraction kernel $|\mathcal{K}|$ is directly proportional to λ. Ideally, a larger contraction kernel is desired as it lowers the height of the pyramid. In absence of the second term in Equation (3), the objective function in Equation (4) might land to a trivial solution with $|\hat{\mathcal{K}}| = 1$ consisting of a single edge $e \in E_k$ with the lowest contrast. In the worse case, for a graph $G_0 = (V_0, E_0)$ at the base level, where $c(e) = 0$ for all edges $e \in E_0$, this will result in a pyramid with height $|V_0|$ and linear complexity for construction of the pyramid (ignoring the pyramid levels required for the removal of the redundant edges) as in (Cerman et al., 2016). Conversely, a larger value of λ will result in a larger size of the contraction kernel, which will eventually reduce the height of the pyramid (ignoring the pyramid levels required for the removal of the redundant edges).

Proposition 1. *If the edges are selected in the ascending order of $\xi(e), \forall e \in E_k$ to construct the contraction kernel $\mathcal{K}$ for $0 < |\mathcal{K}| \leq |E_k|$, then the curve $|\mathcal{K}|$ vs. $\beta(\mathcal{K})$ will not contain any local maximum.*

Proof. The first term $\sum_{j=1}^{|\mathcal{K}|} \xi(e_j)$ of Eq. 3 is a summation of the edges in ascending order of $\xi(e)$. $\xi(e)$ is

bounded between $[0,1]$ as mentioned in Eq. 2. Hence the first term of Eq. 3 will result in a convex curve with no local maximum. The value of the second term $\lambda\left(\frac{|E_k|-|\mathcal{K}|}{|E_k|}\right)$ of Eq. 3 is inversely proportional to the size of the contraction kernel and will result in a linear curve for $0 < |\mathcal{K}| \leq |E_k|$. The sum of both the terms will not result in formation of a local maximum. □
As a consequence of Prop. 1, Eq. 4 is eligible for convex optimization.

Algorithm 1 builds an irregular image pyramid that represents the structure of an image with a graph of critical vertices on its top level.

Algorithm 1: Objective function based selection of the contraction kernel.

1: **Input:** A 2D image P.
2: **Initialize:** Generate the 4-connected neighborhood graph G_0.
3: Insertion of hidden saddle vertices.
4: LBP Categorisation of the vertices into the critical, non-critical and degenerated vertices.
5: **while** #(degenerated vertices) >0 **do**
6: Search for contraction kernel $\hat{\mathcal{K}}$ that optimizes Equation 4.
7: Set the respective critical vertices as the surviving vertices and eliminate the edges connecting two critical vertices from $\hat{\mathcal{K}}$.
8: Contraction of edges $e \in \hat{\mathcal{K}}$.
9: Update the changes in the LBP category of the degenerated vertices.
10: Simplification of graph by removal of redundant multiple edges.
11: **end while**
12: **while** #(non-critical vertices) >0 **do**
13: Search for contraction kernel $\hat{\mathcal{K}}$ that optimizes Equation 4.
14: Set the respective critical vertices as the surviving vertices and eliminate the edges connecting two critical vertices.
15: Contraction of edges $e \in \hat{\mathcal{K}}$.
16: Simplification of graph by removal of redundant multiple edges.
17: **end while**
18: **end**

Theorem 2. *All the faces at the top level of the pyramid built by Algorithm 1 are slope regions.*

Proof. Insertion of the hidden saddles in step 3 of the Algo. 1 converts all the non-well-composed configurations into well-composed c onfigurations. After this step, all the faces in the graph are already slope regions as proven in (Kropatsch et al., 2019)[Proposition 2]. Now the proof boils down to preserving the slope regions without changing the connection of the critical vertices.
For a surface, the topology of its contours changes at the function value of the critical points. For example, the surface contours will collapse to a point at a non-degenerated extremum and multiple contours will intersect at a saddle point. In steps 7 and 14 of Algo. 1, we preserve the critical vertices by fixing them as the surviving vertices and preserve the connection between them by eliminating the edges connecting two critical vertices. Thus all the edges selected for contraction belong to a monotonic path connecting two critical vertices that are not adjacent to each other. Since the monotonic connections between the critical vertices are intact, the topology of the contours will remain the same. Consequently, the slope regions and the topology of the critical vertices are preserved. □

4 DICTIONARY FOR THE CONNECTED COMPONENTS

In this section, we introduce the concept of the dictionary $\mathcal{D}$ for the connected components of the contraction kernel, which comprises sub-graphs conceived as an element of the contraction kernel. The dictionary is particularly designed for implementations with *combinatorial maps* as the data structure. The elements of the dictionary highly depend on the input data, on the application, and on the the data structure used for the implementation. Considering Algorithm 1, the outcome of the algorithm is focused on obtaining the structure of an image, represented as a graph of critical vertices. Since the algorithm operates on an irregular image pyramid, the geometry of the vertices and edges especially in presence of multiple edges and self-loops cannot be captured by the adjacency matrix or adjacency lists. The edge contraction process may subsequently generate a vertex with a higher degree and a complex structure bounded by the complexity of the input data. Therefore, we use combinatorial maps as the data structure, that implicitly encodes and characterizes the inclusion relationships.

Combinatorial pyramids (Brun and Kropatsch, 2001) introduced by Brun *et.* al. is a stack of successively reduced combinatorial maps. It may be understood as explicit encoding of the edge orientation (either in clockwise or anti-clockwise direction) around the vertex. The combinatorial map $M = (D, \sigma, \alpha)$ encoding consists of three components: (a) a set of darts D, (b) a permutation σ and (c) an involution α. An edge e connecting two vertices v, w is composed of two darts d_1, d_2. Darts d_1 and d_2 belonging to the

same edge e, are related to each other by involution α such that $\alpha(d_1) = d_2$ and $\alpha(d_2) = d_1$. The permutation σ relates each dart with the following dart around the same vertex in clockwise or counter-clockwise direction. The direction of encoding is implementation specific. Fig. 3 displays an example of a simple graph encoded as a combinatorial map.

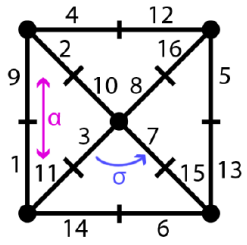

$\mathcal{D}$	1	2	3	4	5	6	7	8	9	10	11	12	13	14	15	16
α	9	10	11	12	13	14	15	16	1	2	3	4	5	6	7	8
σ	14	4	7	9	12	13	8	10	2	3	1	16	15	11	6	5

Figure 3: An example of a simple graph encoded as a combinatorial map.

To maintain generality, the elements of the dictionary are independent of the degree of the vertices and the geometry of the edges at any level of the pyramid. The elements of the dictionary are differentiated based on the contraction ratio defined as the reduction in the number of vertices after contraction of edges in the connected component C. Table 1 enumerates the different classes of the connected components C in the dictionary:

Table 1: Contraction factor for different classes of connected components C in the dictionary $\mathcal{D}$.

$\lvert C\rvert$	contraction factor in $\lvert V_k\rvert$
0	1:1
1	2:1
2	3:1
3	4:1
4	5:1

Fig. 4 displays the graphical representation of the connected components in the dictionary, where the green vertex represents the surviving vertex and the blue colored vertex represents the non-surviving vertices. The solid line edges are the edges selected for the contraction kernel and the dashed lined edges are excluded from the contraction kernel. The solid line edges are oriented from the non-surviving vertex to the surviving vertex, while the dashed line edges are not oriented. The upper bound on the number of the dashed line edges is dependent on the complexity of the data and can be incident to the surviving vertex

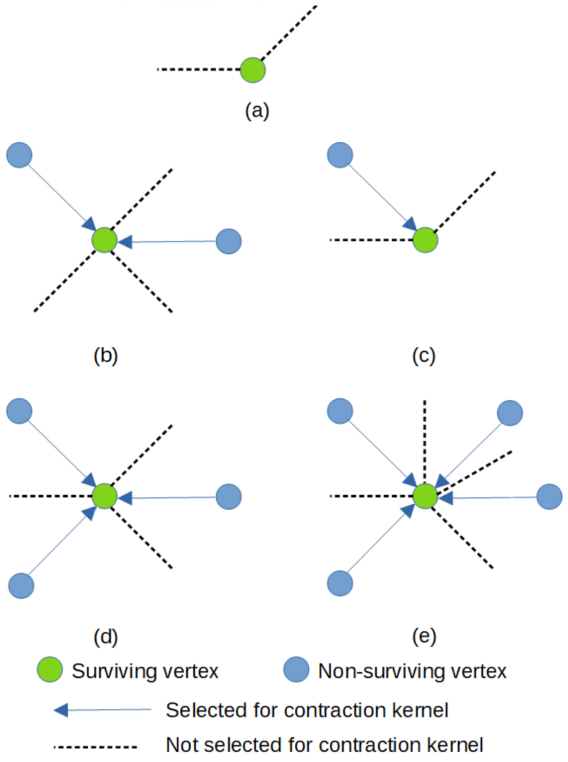

Figure 4: Elements of the dictionary $\mathcal{D}$ for the connected component of the contraction kernel.

at various positions apart from the examples shows in Fig. 4.

Fig.4(a) shows an isolated vertex with respect to the contraction kernel that does not have any incident edges selected for contraction operation. A very common example of an isolated edge is a local extremum surrounded by other critical vertices. In such configurations, none of the edges are selected for contraction.

Fig.4(b) shows a sub-graph with 1 solid edge selected for the edge contraction and 2 dashed edges that are not selected for the contraction. After performing the edge contraction on a single edge of graph $G_k = (V_k, E_k)$, the blue colored vertex will merge with the green vertex creating a new graph $G_{k+1} = (V_{k+1}, E_{k+1})$. The resulting cardinatlity of edge set and vertex set will be as follows: $|E_{k+1}| = E_k - 1$ and $|V_{k+1}| = V_k - 1$ respectively. The similar explanation applies for Fig.4(c),(d) and (e).

Following are the remarks and discussion on the dictionary $\mathcal{D}$:

1. The maximum number of edges selected for the contraction that is incident on a single vertex is 4.
2. A vertex can either be a surviving vertex or a non-surviving vertex. The maximum distance between the surviving vertex of the connected component and the non-surviving vertices is limited to 1.

3. A non-surviving vertex can only have a single surviving vertex. In other words, a single non-surviving vertex cannot have multiple surviving vertices.

The three principal reasons for the above-mentioned remarks are:
(a) At the base level of the pyramid with graph G_0, all the vertices inside the boundary have a degree 4.
(b) Edge contraction operation increases the degree of the surviving vertex and consequently increases the complexity for the removal of the redundant edges (for example: multiple edges and self-loops) for graph simplification. Therefore, contraction of paths (as shown in Fig.5) with more than 1 edges are excluded from the dictionary $\mathcal{D}$. Fig.5(a) shows a subgraph with 2 edges e_1 and e_2 selected for the contraction. The solid green vertex is the single survivor of the connected component. We do not consider bi-colored vertices in our contraction kernels. A bi-colored vertex is a survivor for edge e_2 and a non-survivor for edge e_1. Identifying such paths containing vertices that act as both survivor and non-survivor is linear in complexity and requires expensive computation.
(c) Considering combinatorial maps (Brun and Kropatsch, 2001) as the data structure for all the elements in the dictionary $\mathcal{D}$, the darts incident on a single vertex can be easily traversed by computing the permutations σ starting from a randomly selected dart incident on the surviving vertex. Conversely, the process of identifying a path of contraction kernel is competitively more complicated and time consuming.

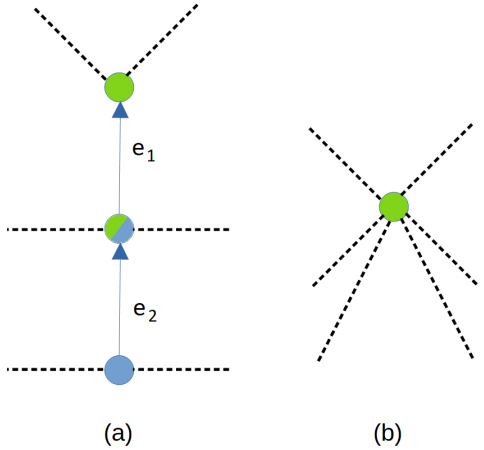

Figure 5: Contraction of a path containing more than 1 edge for contraction, excluded from dictionary $\mathcal{D}$.

5 EXPERIMENTS

This section shows the statistical evidence and experimental verification of the claims made in Section 3. The implementation of the theoretical framework mentioned in this paper can be optimized depending on the application and the data structure in use. To keep the statistics more general and independent of the data-structure, we compared the histogram of $\xi(e)$ in Equation 1 for different values of multiplier m for a total of 400 images randomly selected from the Linnaeus Database (Malmberg et al., 2010). The size of the images are 32×32 (i.e., $|E_0| = 1984$) and the histogram is calculated for $\xi(e), \forall e \in E_0$ of 400 images ($1984 * 400 = 793600$ edges). For the experiments, the contrast of the edges are normalized with respect to the maximum contrast of the image, as required in Eq. 1.

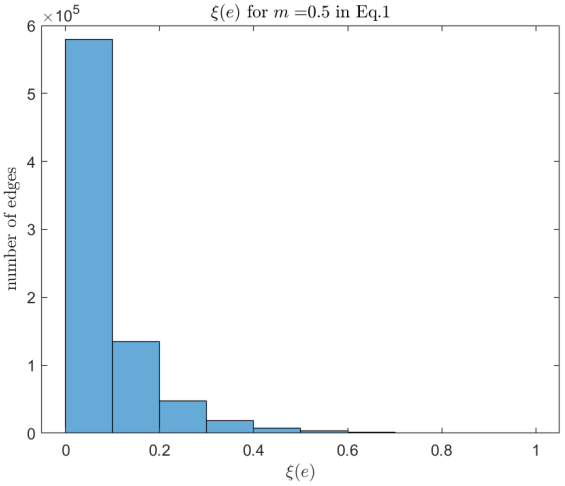

Figure 6: Histogram of $\xi(e)$ for $m = 0.5$ in Eq.1.

From Fig. 6 we can observe that for $m = 0.5$, most of the edges (around 90%) fall in the first two bins with $0 < \xi(e) < 0.2$, while for $m = 1$ and $m = 3$ in Fig. 7,8 there are approximately 75% and 45% of the edges in the first two bins of $\xi(e)$ histogram respectively. It shows that the multiplier m plays a vital role in manipulating the contrast of the edges and set the priority of the edges for the selection process. The results for $m < 0.5$ are not displayed due to lack of visible difference in the histograms. In essence, lower the value of m, higher number of edges will have low cost $\xi(e)$ making them eligible for the selection of the contraction kernel.

Now, let us investigate the cost of the contraction kernel $\beta(\mathcal{K})$ as per Eq. 3 for various values of multiplier m and Lagrange multiplier λ. The graphics displayed in Fig. 9, 11 were computed for a single gray scale im-

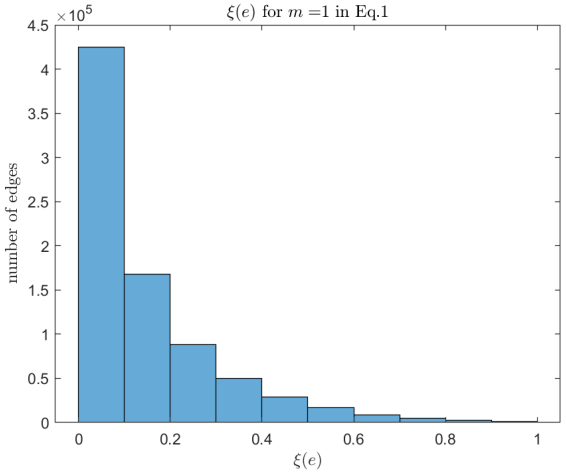

Figure 7: Histogram of $\xi(e)$ for $m = 1$ in Eq.1.

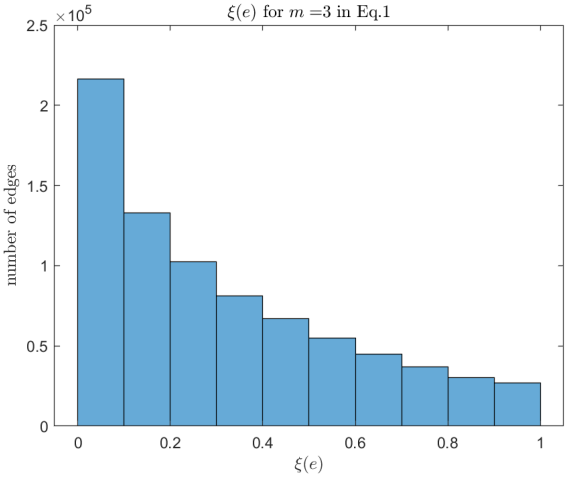

Figure 8: Histogram of $\xi(e)$ for $m = 3$ in Eq.1.

age of size 32×32 containing 1984 edges in E_0. The x-axis represents the size of the contraction kernel $|\mathcal{K}|$ such that the edges are selected in the ascending order of their cost $\xi(e)$ from Eq.1. The red dots mark the minimum values of the curves.The x-coordinate of the red dot corresponds to the $|\hat{\mathcal{K}}|$ and the y-coordinate of the red dot corresponds to the cost of the optimal kernel $\beta(|\hat{\mathcal{K}}|)$. Each figure contains curves for different value of $m = 0.15, 0.12, 0.09, 0.06, 0.03$ and a single value of λ.

On detailed observation of the above graphs and the corresponding value of $\xi(e), \forall e \in \mathcal{K}$, following were our observations:

1. At the initial stage of the pyramid, $\hat{\mathcal{K}}$ comprises edges with $\xi(e) > 0$ i.e. edges that are not a part of plateau regions and level curves. This is explicitly displayed by the orange curve in Fig.11 with $m = 0.03$ and $\lambda = 16$. The minimum value of the curve $\beta(\mathcal{K})$ is attained at $|\mathcal{K}| = 1700$ edges (ap-

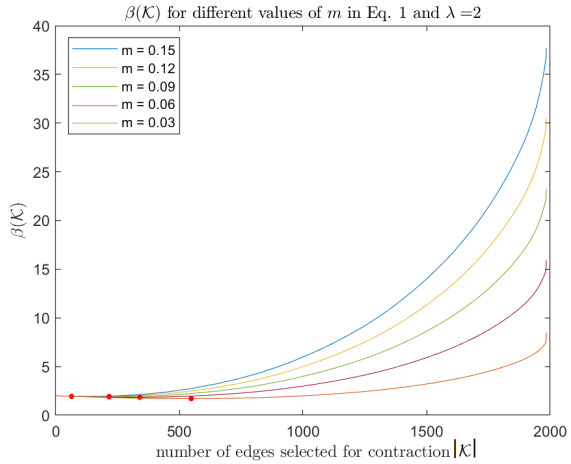

Figure 9: Number of edges selected for the contraction kernel $|\mathcal{K}|$ vs. cost of the contraction kernel $\beta(\mathcal{K})$ for $\lambda = 2$.

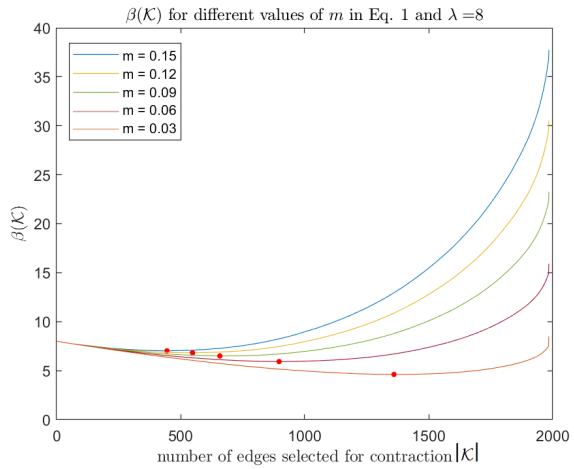

Figure 10: Number of edges selected for the contraction kernel $|\mathcal{K}|$ vs. cost of the contraction kernel $\beta(\mathcal{K})$ for $\lambda = 8$.

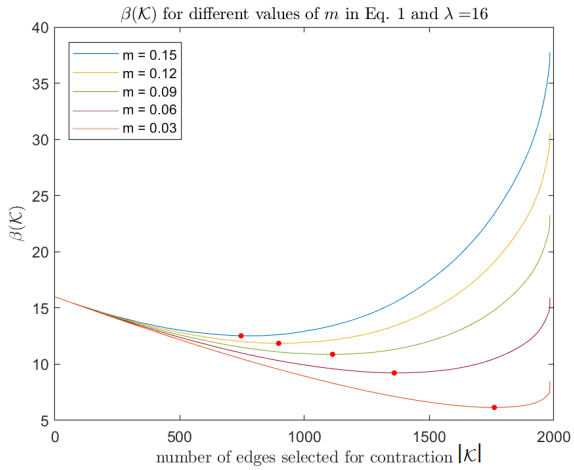

Figure 11: Number of edges selected for the contraction kernel $|\mathcal{K}|$ vs. cost of the contraction kernel $\beta(\mathcal{K})$ for $\lambda = 16$.

proximately). As a result there is a higher chance of the edges with a higher contrast to be selected for the contraction kernel. This may change the topology of the image if step 7 and 14 of Algo.1 are not followed. A large size of the contraction kernel will eventually increase the complexity for the removal of the edge and graph simplification.

2. For a lower value of λ (typically < 2) and a short range of $0 < m < 1$, the minimum of all the curves $\beta(\mathcal{K})$ for different values of m are very close to each other and tend to result in the selection of the same contraction kernel. Fig. 9 is a good example where only 4 minima are visible because the red marker for the minimum for curve $m = 0.12$ and $m = 0.09$ coincide each other. Conversely, with a higher value of λ (typically > 10), we can easily differentiate between the minimum of the curves as displayed in Fig. 10,11.

5.1 Estimating the Original Image from a Blurred Binary Image

In this experiment, we used the proposed method for estimating the original binary image from its blurred version utilizing the concept of connected component labelling (CCL). We assume that the edges present in the interior of a component will have a lower contrast as compared to the edges connecting two distinct components. By varying the value of the multiplier m and λ in Eq. 3, we managed to obtain a contraction kernel containing edges connecting two components with a small contrast. In Fig. 12, to display an easily observable and intuitive result, we generated an artificial image. Fig. 12a shows an image after Gaussian blur with standard deviation of 0.6 while Fig. 12b displays CCL with 126 components for $m = 0.15$ and $\lambda = 15$ and $|\hat{\mathcal{K}}| = 76.26\%$ of total edges. By further reducing the value of m to 0.05 and increasing the value of λ to 25, we modify $\xi(e)$ such that higher number of edges are eligible for the contraction kernel and $|\hat{\mathcal{K}}| = 77.6\%$ of the total edges. As a result the number of connected components reduce to 66 as displayed in Fig. 12c. Repeating the process further, by lowering m to 0.01 and increasing λ to 45, the number of edges eligible for contraction raise to $|\hat{\mathcal{K}}| = 92.7\%$, resulting in 6 connected components corresponding to the original binary image as shown in Fig. 12d.

The experiments of connected component labelling were performed on the YACCLAB database (Grana et al., 2016). Fig. 13 shows the results of deblurring MRI binary image from YACCLAB database. Fig. 13b shows the CCL on the original image with 1070 connected components. Fig. 13c and Fig. 13d shows the CCL on the deblurred images resulted after tuning the values of m and λ. With $m = 0.01$ and $\lambda = 100$, we achieved a slight deblurring but the number of connected components were still high around 12155 as shown in Fig. 13c. With further fine tuning the values- $m = 0.008$ and $\lambda = 200$, we achieved a better deblurred image with 2642 number of connected components (refer Fig. 13d). Table 3 summarizes the results displayed in Fig. 13. From our observations, the deblurring was not optimal for higher amount of Gaussian blurring especially when the small connected components were placed to each other.

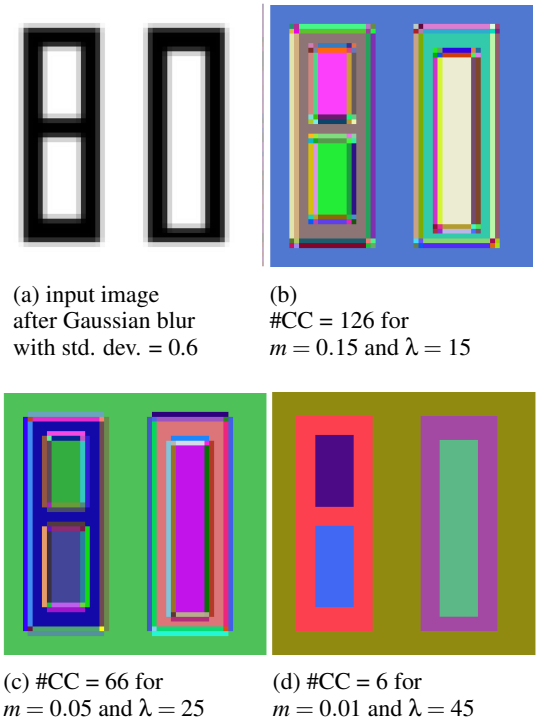

(a) input image after Gaussian blur with std. dev. = 0.6

(b) #CC = 126 for $m = 0.15$ and $\lambda = 15$

(c) #CC = 66 for $m = 0.05$ and $\lambda = 25$

(d) #CC = 6 for $m = 0.01$ and $\lambda = 45$

Figure 12: Connected component labelling of blurred binary image with different value of parameter m and λ.

Table 2: Values of parameter m, λ and the resulting number of connected components for Fig. 12a.

output	m	λ	number of connected components (#CC)
Fig. 12b	0.15	15	126
Fig. 12c	0.05	25	66
Fig. 12d	0.01	45	6

The experiments performed on the YACCLAB database (Grana et al., 2016) are available: "click here" (or visit: https://www.prip.tuwien.ac.at/people/darshan/more/publications/9_TR.pdf). The documented results display both desirable and undesirable results for connected component labelling and deblurring of binary images.

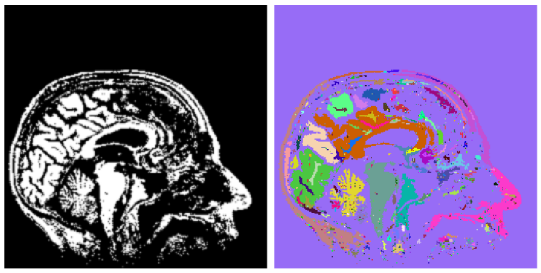

(a) input image after Gaussian blur with std. dev. = 0.6

(b) CCL of original image #CC = 1070 for $m = 0.05$ and $\lambda = 90$

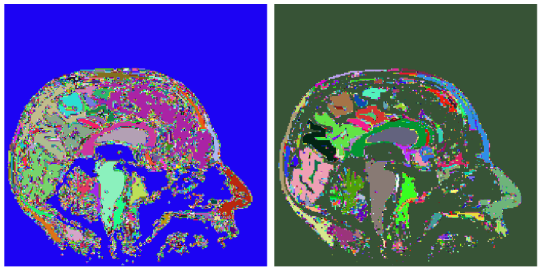

(c) #CC = 12155 for $m = 0.01$ and $\lambda = 100$

(d) #CC = 2642 for $m = 0.008$ and $\lambda = 200$

Figure 13: Connected component labelling of blurred binary image with different value of parameter m and λ

Table 3: Values of parameter m, λ and the resulting number of connected components for Fig. 13a.

output	m	λ	number of connected components (#CC)
Fig. 13b	0.05	90	1070
Fig. 13c	0.01	100	12155
Fig. 13d	0.008	200	2642

Remarks: We observe that given a dataset of blurred images, the values of parameter m and λ can be learned to achieve an optimal deblurring of a test sample with similar amount of blurring.

As per the TIIP algorithm mentioned (Batavia et al., 2020), the plateau regions are contracted before classification of the vertices followed by the contraction of the edges with $c(e) > 0$, while preserving the critical points. Assume we have a 2D image P with R as the plateau region with the largest diameter d_R and C as the gray scale region with the largest diameter d_C after contraction of R. Then the computational complexity of this algorithm for construction of an irregular pyramid is $O(log(d_R)+log(d_C))$. With the help of the objective function we can further reduce the complexity, since we can contract the edges with $c(e) > 0$ simultaneously with the contraction of the plateau region. Thus the complexity is reduced to $O(log(d_{CC}))$ where d_{CC} corresponds to the diameter of the largest connected component that may include the gray scale region C and the plateau region R.

6 CONCLUSIONS

The paper introduces a novel approach for the selection of the contraction kernel using an objective function. We proved that the proposed algorithm based on the objective function navigates the construction of the irregular pyramid to decompose a 2D image into monotonically connected image surface regions (slope regions). The objective function attempts to replicate the TIIP algorithm mentioned in (Batavia et al., 2020; Gonzalez-Diaz et al., 2021) and enables easier modifications for application-oriented results. It can be envisioned as a step towards learning the contraction kernel for the construction of an irregular image pyramid. Later we showed statistical observations that assist in tuning the parameter values of the objective function. The experiments were focused on deblurring of blurred images to recover the original binary image and connected component labelling. Lastly, the paper establishes the concept of the dictionary of the connected components of the contraction kernel. This dictionary is similar to the dictionary of the shapes but instead is designed for the graphs especially considering combinatorial maps as the data structure. The elements of the dictionary can be used for the optimization of the objective function and to realize the solution for the decomposition of an image. We leave the optimization method and the grammar of connected components for future research.

7 FUTURE WORK

The objective function in Equation 4 revolves around the contrast of an edge. However, it does not help with the location of the edges in binary images or with plateau regions, since the contrast of edges belonging to the same component in a binary image (or plateau regions) is zero. Edges with same contrast have the equal priority as per the proposed objective function. We intend to produce a grammar of the contraction kernel that repeats its occurrence to deliver an easy solution. Fig. 14 shows an example of a 9×9 grid like structure of the plateau region such that the solid and the dashed lines correspond to the edges and the crossing of the lines correspond to the vertices. All the edges e have the same contrast $c(e) = 0$. The set of the oriented edges form the contraction kernel and the edges are oriented from the non-surviving vertex

to the surviving vertex. The position of the surviving vertex forms a pattern that corresponds to the knight's move in chess. This repetition ensures that the connected components are independent and upon contraction, it results in a rotated version of the grid like structure as shown in Fig.15. The grammar can be reused on higher levels until the grid structure exists. Computation of redundant edges, double edges in our case as shown in Fig.15 can be pre-computed without an expensive search.

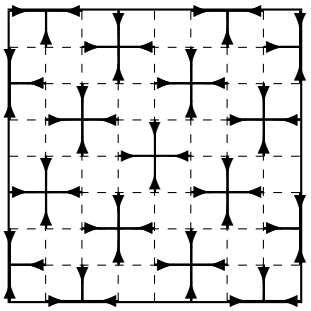

Figure 14: Knight's vertex contraction kernel for 9×9 plateau region.

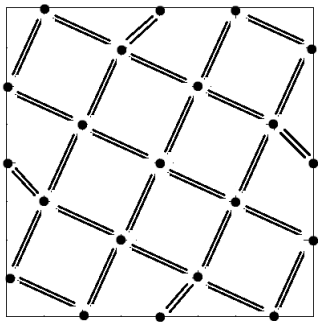

Figure 15: After contraction of Knight's vertex contraction kernel for 9×9 plateau region..

Similar to the graph edit distance, we can compute the pyramid edit distance for an irregular image pyramid, based on the cost of the contraction kernel at each level.

REFERENCES

Batavia, D., González-Díaz, R., and Kropatsch, W. G. (2020). Image = structure + few colors. In *Structural, Syntactic, and Statistical Pattern Recognition - Joint IAPR Int. Workshops, S+SSPR*, LNCS, pages 365–375. Springer.

Batavia, D., Hladůvka, J., and Kropatsch, W. G. (2019). Partitioning 2D Images into Prototypes of Slope Region. In *Int. Conference on Computer Analysis of Images and Patterns*, LNCS, pages 363–374. Springer.

Brun, L. and Kropatsch, W. (2001). Introduction to combinatorial pyramids. In *Digital and image geometry*, pages 108–128. Springer.

Cerman, M., Janusch, I., Gonzalez-Diaz, R., and Kropatsch, W. G. (2016). Topology-based image segmentation using LBP pyramids. *Machine Vision and Applications*, 27(8):1161–1174.

Comic, L., De Floriani, L., and Iuricich, F. (2010). Building Morphological Representations for 2D and 3D Scalar Fields. In Puppo, E., Brogni, A., and Floriani, L. D., editors, *Eurographics Italian Chapter Conference 2010*, pages 103–110.

Edelsbrunner, H., Harer, J., and Zomorodian, A. (2003). Hierarchical morse-smale complexes for piecewise linear 2-manifolds. *Discrete and computational Geometry*, 30(1):87–107.

Gonzalez-Diaz, R., Batavia, D., Casablanca, R. M., and Kropatsch, W. G. (2021). Characterizing slope regions. *Journal of Combinatorial Optimization*, pages 1–20.

Grana, C., Bolelli, F., Baraldi, L., and Vezzani, R. (2016). YACCLAB - Yet Another Connected Components Labeling Benchmark. In *23rd International Conference on Pattern Recognition*. ICPR.

Gyulassy, A., Günther, D., Levine, J. A., Tierny, J., and Pascucci, V. (2014). Conforming Morse-Smale Complexes. *IEEE Transactions on Visualization and Computer Graphics*, 20(12):2595–2603.

Helman, J. L. and Hesselink, L. (1991). Visualizing vector field topology in fluid flows. *IEEE CGA*, 11(3):36–46.

Kropatsch, W. G., Casablanca, R. M., Batavia, D., and Gonzalez-Diaz, R. (2019). On the space between critical points. In *Int. Conference on Discrete Geometry for Computer Imagery*, LNCS, pages 115–126. Springer.

Latecki, L., Eckhardt, U., and Rosenfeld, A. (1995). Well-composed sets. *Comput. Vis. Image Underst.*, 61:70–83.

Lee, R. N. (1984). Two-dimensional critical point configuration graphs. *IEEE Transactions on Pattern Analysis and Machine Intelligence*, (4):442–450.

Malmberg, G., Nilsson, L.-G., and Weinehall, L. (2010). Longitudinal data for interdisciplinary ageing research. design of the linnaeus database. *Scandinavian journal of public health*, 38(7):761–767.

Morales-González, A. and García-Reyes, E. B. (2013). Simple object recognition based on spatial relations and visual features represented using irregular pyramids. *Multimedia tools and applications*, 63(3):875–897.

Shinagawa, Y., Kunii, T., and Kergosien, Y. (1991). Surface coding based on morse theory. *IEEE Computer Graphics and Applications*, 11(5):66–78.

Stein, E., Milnor, J. W., Spivak, M., Wells, R., Wells, R., and Mather, J. N. (1963). *Morse Theory*. Princeton University Press.